J. Fluid Mech. (2002), *vol.* 456, *pp.* 33–48. © 2002 Cambridge University Press
DOI: 10.1017/S0022112001007303 Printed in the United Kingdom

A laboratory study of the velocity structure in an intrusive gravity current

By RYAN J. LOWE, P. F. LINDEN AND JAMES W. ROTTMAN

Department of Mechanical and Aerospace Engineering, University of California, San Diego, 9500 Gilman Drive, La Jolla, CA 92093-0411, USA

(Received 7 November 2000 and in revised form 7 September 2001)

Laboratory experiments were performed in which an intrusive gravity current was observed using shadowgraph and particle tracking methods. The intrusion was generated in a two-layer fluid with a sharp interface by mixing the fluid behind a vertical lock gate and then suddenly withdrawing the gate from the tank. The purpose of the experiments was to determine the structure of the velocity field inside the intrusion and the stability characteristics of the interface. Soon after the removal of the lock gate, the front of the intrusive gravity current travelled at a constant speed close to the value predicted by theory for an energy-conserving gravity current. The observed structure of the flow inside the intrusion can be divided into three regions. At the front of the intrusion there is an energy-conserving head region in which the fluid velocity is nearly uniform with speed equal to the front speed. This is followed by a dissipative wake region in which large billows are present with their associated mixing and in which the fluid velocity is observed to be non-uniform and have a maximum speed approximately 50% greater than the front speed. Behind the wake region is a tail region in which there is very little mixing and the velocity field is nearly uniform with a speed slightly faster than the front speed.

1. Introduction

A gravity current is the mainly horizontal, buoyancy-driven motion of a fluid of one density into a fluid of another density. Gravity currents occur frequently in geophysical and industrial flows. A comprehensive description of gravity currents and their numerous applications is given in Simpson's (1997) book. In this paper we investigate a type of intrusive gravity current that flows along the interface between two fluid layers of different densities and has a density between that of the two layers.

More specifically, we investigate the type of intrusive gravity current that is produced by a full-depth lock release in a tank containing two equal-depth layers of fluids of different densities. This type of flow is generated by inserting a vertical barrier (the lock gate) into the tank and then mixing the fluid on one side of the barrier (the lock) to produce a fluid with a uniform density that is approximately the average of the two layers. The intrusion generated when the barrier is withdrawn from the tank is found to be symmetric about the interface between the two layers and to occupy approximately half the depth of each layer. Previous observations, as described for example by Britter & Simpson (1981), have shown that these intrusions advance initially at a constant speed. Holyer & Huppert (1980) and de Rooij, Linden & Dalziel (1999) have shown that these types of symmetric intrusions can

https://doi.org/10.1017/S0022112001007303 Published online by Cambridge University Press

be described by a straightforward generalization of Benjamin's (1968) theory for an energy-conserving boundary gravity current. Indeed, for Boussinesq flows (e.g. salt water advancing into fresh water) the intrusion is identical to two boundary gravity currents that are travelling together on either side of the interface.

Benjamin (1968) proposed a theory for steadily advancing gravity currents that flow along a solid horizontal boundary. This theory gives a relationship between the front speed and the far-downstream depth of the gravity current. For the special case of an energy-conserving gravity current, the theory predicts that the current occupies half the depth of the tank. Also, for this special case, Benjamin (1968) derived an approximate expression for the shape of the current.

Benjamin's theory, strictly speaking, is for an empty cavity advancing into a liquid. To apply his theory to Boussinesq currents it is necessary to assume that there is no mixing between the current and the surrounding fluid and that there is no net relative flow within the current. In reality, however, neither of these assumptions is true. Mixing is observed to occur in Boussinesq gravity currents due to the formation of billows on the interface separating the fluids. Mixing results when the billows grow in size and subsequently collapse behind the gravity current 'head' region. As a consequence, the velocity cannot be uniform within a gravity current. Simpson & Britter (1979) conducted experiments on a boundary gravity current, and showed that there is a relative forward velocity behind the steadily advancing front, which supplies the volume flux necessary to balance the losses from the current due to mixing. They found, based on mean volume flux measurements, that there is an internal flow within the current characterized by a mean 'overtaking speed' of about 15% greater than the front speed.

Despite the obvious mixing in the wake region, the present experiments as well as previous full-depth lock-release gravity current experiments, such as those described in Rottman & Simpson (1983), and the direct numerical simulations of Härtel, Meiburg & Necker (2000), reveal that Benjamin's energy-conserving theory accurately predicts the front speeds and current heights. The success of Benjamin's theory implies that the dynamics of a gravity current front are not greatly affected by the mixing processes nor the internal flow within the current. The objective of the present paper is to gain some insight into why mixing plays such a minor role in gravity current frontal dynamics.

To achieve this objective, we performed an experimental study of the velocity field in intrusive gravity currents produced by full-depth lock releases. We obtained detailed measurements of the two-dimensional velocity structure within symmetric intrusive gravity currents using digital particle tracking velocimetry. Each velocity field was compared with a corresponding shadowgraph image to relate the velocity structure to the mixing processes.

The results of our experiments reveal that the intrusion can be divided into three flow regions. There is a 'head region' at the front of the current in which the velocity is nearly uniform and has approximately the same speed as the front itself. This is followed by a wake region in which there is billow formation and associated mixing. In this region the velocity field is non-uniform and speeds can be as high as 50% greater than the front speed. Behind the wake region is a tail region in which there is very little mixing and the velocity field is nearly uniform with a speed slightly faster than the front speed.

This description of the intrusion velocity field contradicts the accepted model, as described for example in Simpson (1997). In this model fluid from the rear of the gravity current propagates all the way to the front where it flows back along the

https://doi.org/10.1017/S0022112001007303 Published online by Cambridge University Press

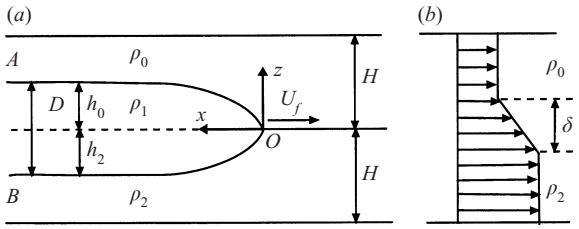


FIGURE 1. (*a*) A sketch of an intrusion front defining the nomenclature used in the text. (*b*) A typical vertical density profile, in which δ represents the thickness of the interface.

current interface and then mixes with the ambient fluid in the billow structures that form in the wake of the head region. Our description shows that most of the fluid from the rear of the gravity current propagates to just behind the head where it mixes with the ambient fluid leaving the head region largely unaffected.

Some previous experimental results are consistent with our description of the interior flow in a gravity current. Measurements of the density field in gravity currents by Hallworth *et al.* (1996) and Hacker, Linden & Dalziel (1996) show that the fluid within the head of a gravity current produced by a fixed-volume release does not change significantly during the constant speed phase. However, these studies did not measure the velocity field inside the gravity current.

In § 2 we derive the theoretical front speed and current heights for an energy-conserving intrusion with small relative density differences. The experimental procedure is described in § 3, and the results from the experiments are presented and discussed in § 4. In § 4 we also compare our experimental measurements to the velocity structure Härtel *et al.* (2000) observed in their two-dimensional simulations with free-slip boundary conditions. Finally, § 5 includes a summary of the findings and the major conclusions drawn from the experiments.

2. Theory

A schematic diagram of an intrusive gravity current with front speed U_f and total thickness D flowing along the interface between two fluid layers, each of equal depth H, is shown in figure 1. The lower layer fluid has density ρ_2 and the upper layer fluid has density ρ_0, with $\rho_2 > \rho_0$, and it is assumed that the interface thickness δ between the layers is infinitely thin (i.e. $\delta \approx 0$). The density ρ_1 of the fluid within the intrusion is taken to be the average of the densities in the two layers: $\rho_1 = (\rho_0 + \rho_2)/2$. The downstream intrusion heights relative to upstream interface position are h_0 in the top layer and h_2 in the bottom layer.

Given H, ρ_0 and ρ_2, we seek expressions for h_0, h_2 and U_f. Following the analysis of Holyer & Huppert (1980), de Rooij *et al.* (1999) applied mass conservation in each layer of ambient fluid and, assuming the flow to be energy-conserving, applied Bernoulli's equation along streamlines OA and OB, to derive relationships in each layer between the intrusion front speed U_f and the downstream intrusion heights h_0 and h_2,

$$U_f^2 = 2g_0' h_0 \left(\frac{H^2}{(H-h_0)^2} + \frac{g_0'}{g} \right)^{-1} \tag{2.1}$$

$$U_f^2 = 2g_2' h_2 \left(\frac{H^2}{(H-h_2)^2} - \frac{g_2'}{g} \right)^{-1}, \tag{2.2}$$

where the reduced gravities are defined by $g_0' = g(\rho_1 - \rho_0)/\rho_0$ and $g_2' = g(\rho_2 - \rho_1)/\rho_2$.

https://doi.org/10.1017/S0022112001007303 Published online by Cambridge University Press

Since in this case $\rho_1 = \frac{1}{2}(\rho_0 + \rho_2)$, these reduced gravities can be simplified to $g_0' = \frac{1}{2}g(\gamma^{-1} - 1)$ and $g_2' = \frac{1}{2}g(1 - \gamma)$, where $\gamma = \rho_0/\rho_2$ is the density ratio between the upper and lower layers.

For Boussinesq fluids $g_0'/g \approx g_2'/g \approx 0$, so equations (2.1)–(2.2) can be approximated as

$$U_f = \sqrt{2g_0'h_0}\left(1 - \frac{h_0}{H}\right), \tag{2.3}$$

$$U_f = \sqrt{2g_0'h_2}\left(1 - \frac{h_2}{H}\right). \tag{2.4}$$

Since these two expressions must be equal, $h_0 = h_2$. Benjamin (1968) found that a gravity current flowing over a rigid boundary is energy-conserving only if it fills one-half of the tank. We expect that an energy-conserving intrusion will similarly be half-depth in each of the ambient layers, so that

$$h_0 = h_2 = \frac{H}{2}. \tag{2.5}$$

Substitution of these intrusion heights into the integral momentum conservation equation (equation (7) in de Rooij *et al.* 1999) reveals that this is indeed the case. Finally, substituting (2.5) into (2.3) and (2.4) gives an expression for the non-dimensional front speed

$$Fr = \frac{U_f}{\sqrt{g_0'H}} = \frac{1}{2}, \tag{2.6}$$

where Fr is the Froude number. This is identical to the result Benjamin (1968) obtained for an energy-conserving boundary gravity current if the upstream interface depth is taken as the solid boundary (the lower boundary in the upper layer and the upper boundary in the lower layer).

This analysis assumes that the interface is infinitely thin and the fluid layers are Boussinesq. In our experiments both the interface thickness and the density differences between the layers are finite.

Britter & Simpson (1981) and Faust & Plate (1984) investigated the effect of the interface thickness in symmetric Boussinesq intrusions and observed that both the front speed and the intrusion heights decrease as δ increases. As the ratio of δ to the intrusion thickness D is increased, the strength of the billows is reduced and mixing between the fluid layers is suppressed. For interface thickness ratios less than $\delta/D \approx 0.2$ they determined that an intrusive gravity current behaves very similarly to an intrusion travelling along an infinitely thin interface. For values of the interface thickness ratio above 0.2, the properties of the intrusion were a function of this ratio. At a critical ratio $\delta/D \approx 1$, the mixing between the fluid in the intrusion and the surrounding fluid is completely suppressed. All of the experiments described in this paper are for intrusive gravity currents with interface thickness ratios well under 0.2.

The effects of non-Boussinesq density ratios are discussed in the Appendix. For the range of densities in our experiments these effects are shown to be very small.

3. Experimental procedure

3.1. *Filling of the tank and generation of intrusions*

A schematic of the experimental apparatus is shown in figure 2. The experiments were performed in a rectangular Plexiglas tank of 182 cm length, 23 cm width and

https://doi.org/10.1017/S0022112001007303 Published online by Cambridge University Press

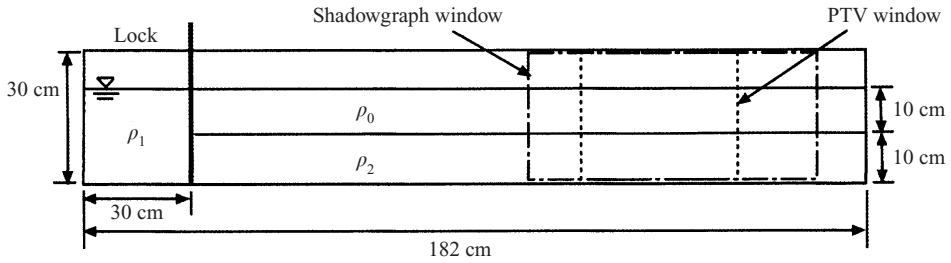


FIGURE 2. The experimental setup before the intrusion is released into a two-layer fluid.

30 cm depth. The tank was first filled to a depth of 10 cm with salt water of density ρ_2. A 10 cm layer of fresh water of density ρ_0 was then carefully added on top of the saline layer, using a porous float to reduce mixing. The interface thickness was measured from the shadowgraphs using a ruler and was less than 1.5 cm in all cases, so that all experiments were performed on intrusions with effectively sharp interfaces. Once filled, a vertical gate was inserted a distance of 30 cm from one end of the tank to form a lock and the fluid behind the gate was mixed to an average density $\rho_1 \approx (\rho_0 + \rho_2)/2$. Densities were measured with an ANTON PAAR DMA 500 density meter with an accuracy of $\pm 10^{-5}\,\mathrm{g\,cm^{-3}}$. To start the experiment, the gate was smoothly withdrawn vertically, causing the fluid in the lock to flow along the interface as an intrusive gravity current. The intrusions were observed by using either a shadowgraph to visualize the density field or particle tracking velocimetry (PTV) to quantify the velocity field.

3.2. *Shadowgraph visualization*

The shadowgraphs were obtained by covering the front of the tank with a sheet of drafting vellum and positioning a 300 W slide projector 4 m behind the tank. The shadowgraph was photographed every 0.25 s using a 35 mm camera, and was also recorded with a COHU 4912 CCD camera onto super-VHS video tape. The video window was 60 cm wide and its downstream end was located 10 cm from the endwall, as shown in figure 2. The image-processing software DigImage was used to process the recordings off-line and the front speed and current heights for each intrusion were calculated.

3.3. *Particle visualization*

For PTV, the fluid in the lock was seeded with approximately 4.5 g of particles of Pliolite VT, an opaque resin with an average density of $1.022\,\mathrm{g\,cm^{-3}}$. The particles were sieved to have diameters between 425 and 600 μm and were soaked in a wetting agent to reduce the effect of surface tension. The particles were illuminated by the light from a slide projector placed 3 m behind the tank. The light was reflected up through the bottom of the tank by a mirror at a 45° angle to the horizontal, as shown in figure 3. A 1.5 cm wide vertical sheet of light was created in the centre of the tank by covering sections of the bottom of the tank. The motion of the particles was imaged by the CCD camera and recorded onto a video tape. The video window was 30 cm wide and its downstream end was located 30 cm from the endwall, as shown in figure 2. This window overlapped with a section of the shadowgraph window, allowing the two images (from separate experiments) to be matched. The DigImage software was used to track the particles and calculate the flow velocities. Approximately 500

https://doi.org/10.1017/S0022112001007303 Published online by Cambridge University Press

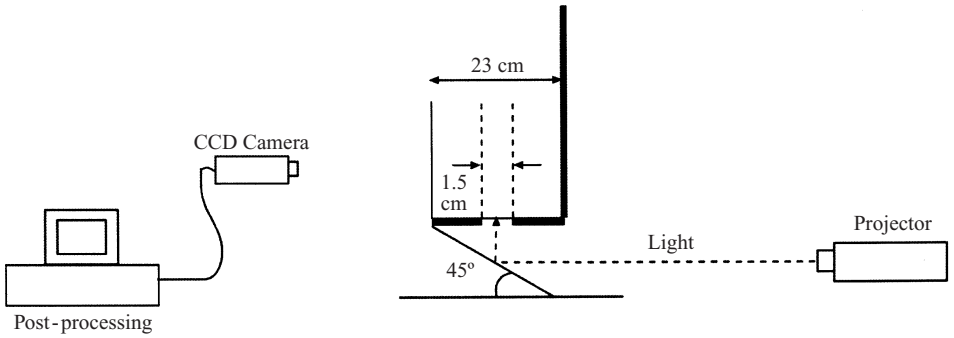


FIGURE 3. The lighting arrangement used during PTV.

Run	ρ_0 ($\mathrm{g\,cm^{-3}}$)	ρ_2 ($\mathrm{g\,cm^{-3}}$)	g_0' ($\mathrm{cm\,s^{-2}}$)	Fr	ϕ	Re_H
PTV Runs						
A	1.0164	1.0287	5.955	0.474	0.472	3700
B	1.0085	1.0306	10.783	0.462	0.424	4800
C	1.0044	1.0363	15.604	0.493	0.437	6200
D	1.0029	1.0399	18.081	0.476	0.451	6400
E	0.9985	1.0465	23.615	0.488	0.451	7500
F	0.9867	1.0544	33.627	0.467	0.431	8600
Shadowgraph Runs						
G	1.0081	1.0308	11.040	0.494	0.451	5200
H	1.0026	1.0399	18.248	0.494	0.466	6700
I	1.0028	1.0406	18.507	0.493	0.488	6700
J	0.9982	1.1822	90.531	0.483	0.465	14500

TABLE 1. Experimental parameters.

particles were tracked in each video frame and the velocity field was determined at points on either a 16×32 or 20×40 grid, depending on the run.

In order to minimize the refraction of light due to the mixing of the different fluids, it was necessary to match their refractive indices. For this purpose, a small amount of 2-propanol was added to the fresh water layer, which changed its refractive index. The refractive indices were measured using an ATAGO Palette PR-101 digital refractometer. The addition of 2-propanol, which has a density of $0.785\,\mathrm{g\,cm^{-3}}$, slightly reduced the density of the light fluid layer. To ensure that the particles were approximately neutrally buoyant, densities ρ_0 and ρ_2 were selected such that the fluid of density ρ_1 within the intrusion closely matched the $1.022\,\mathrm{g\,cm^{-3}}$ density of the Pliolite. As a result, it was necessary to add some salt to the upper layer to raise its density above that of fresh water.

A total of 10 experiments were conducted with parameters listed in table 1, corresponding to four shadowgraph runs and six PTV runs. The range of Reynolds numbers $Re_H = U_f H/\nu$ is between 3700 and 14 500, where U_f is the front speed, H is half the total fluid depth in the tank and ν is the kinematic viscosity of fresh water. These Reynolds numbers are well above the value $Re_H \approx 2000$ Simpson & Britter (1979) determined for Reynolds number independence for boundary gravity currents.

https://doi.org/10.1017/S0022112001007303 Published online by Cambridge University Press

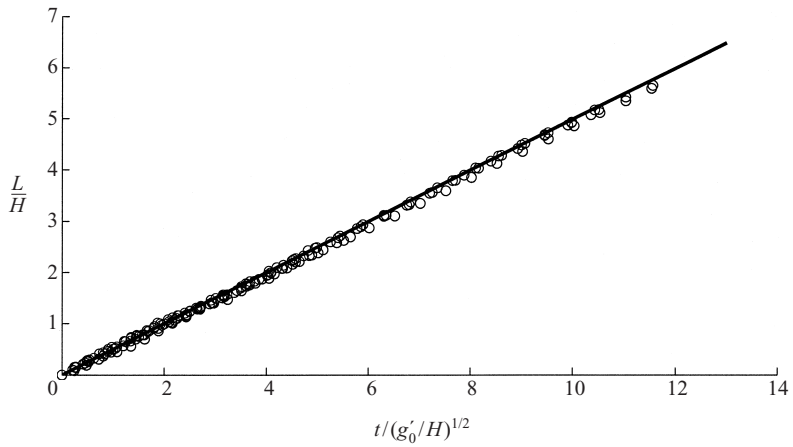


FIGURE 4. The length L of the intrusion in the video window as a function of the time t since the intrusion first entered the window, for all experiments listed in table 1. The straight line has slope equal to the energy-conserving front speed given by (2.6).

4. Results and discussion

4.1. *Front speeds and current heights*

Figure 4 shows the intrusion length L scaled by H as a function of time scaled by $(g_0'/H)^{1/2}$ for all experiments. The time $t = 0$ is set to the time when the intrusion first enters the video window. Figure 4 shows that the front speed of each intrusion was constant during the period it passed through the video window. The solid line in this plot has a slope corresponding to the energy-conserving front speed given by (2.6), and the agreement with the experimental values is within the resolution of the measurements.

Table 1 lists the measured Froude numbers Fr and dimensionless intrusion thicknesses $\phi = D/2H$. These values show no systematic variation with Re_H, and are only a few percent lower than the theoretical energy-conserving values $Fr = 1/2$ and $\phi = 1/2$. This deviation from the energy-conserving values is at least partially due to the finite thickness of the interface, which has been shown by Faust & Plate (1984) to reduce slightly both Fr and ϕ. Thus for all of the intrusions in these experiments, Benjamin's energy-conserving theory accurately predicts the front speeds and current thicknesses, despite the observed dissipative mixing in the wake region of the intrusions.

4.2. *Two-dimensional velocity structures and current shapes*

Contours of the instantaneous horizontal and vertical velocity components, u and v, respectively, nondimensionalized by the front speed U_f, are presented in figure 5. Results for two different Reynolds numbers are shown corresponding to Run B ($Re_H = 4800$) in figure 5(*a*,*c*) and Run F ($Re_H = 8600$) in figure 5(*b*,*d*). The contour scale for the horizontal velocity components only includes dimensionless velocities $U/U_f > 1$ to emphasize the horizontal velocities moving faster than the front speed. Each example shows a region of high-speed fluid, beginning at $x/H \approx 1.5$, where x is the distance behind the intrusion front, and extending throughout the rear of the intrusion. In this region the horizontal velocities are approximately 30% to 50% faster than the front speed. However, from $x/H \approx 0$ to 1, in the region corresponding

https://doi.org/10.1017/S0022112001007303 Published online by Cambridge University Press

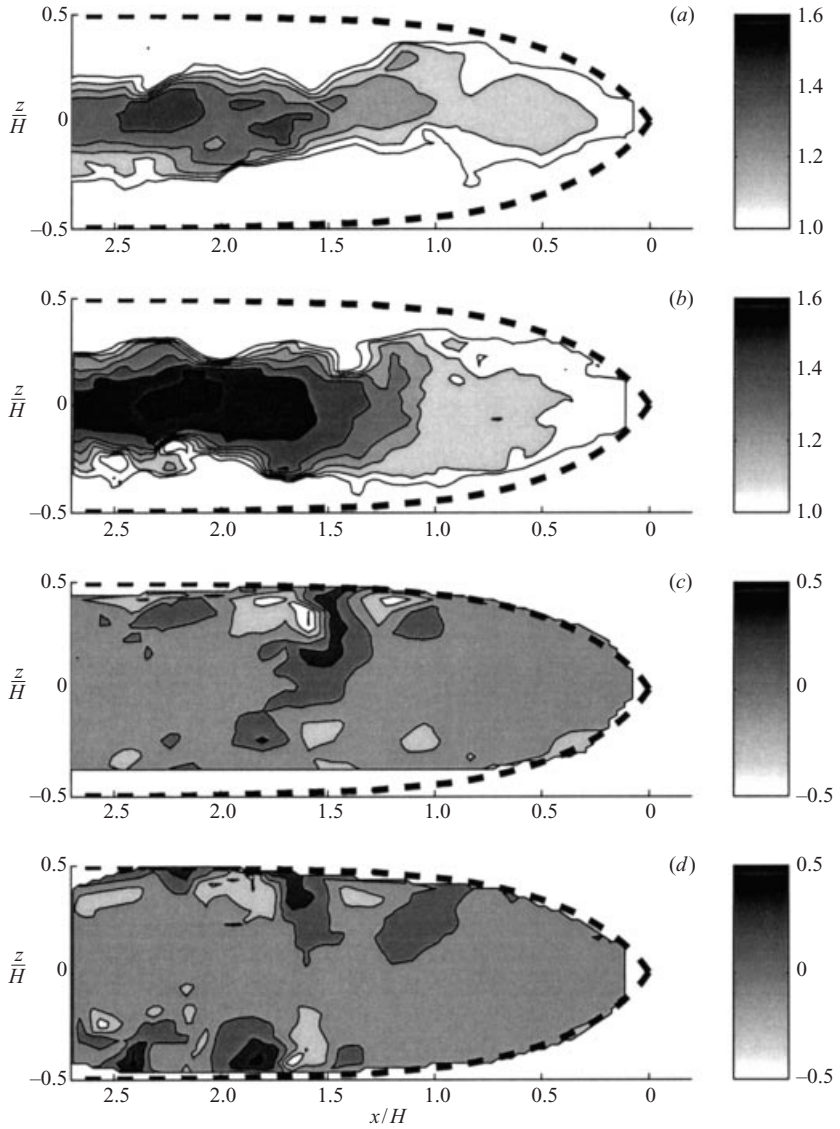


FIGURE 5. (*a*,*b*) Contour maps of the horizontal velocity for Run B ($Re_H = 4800$) and Run F ($Re_H = 8600$), respectively. (*c*,*d*) Corresponding contours of the vertical velocity. The contour interval for the horizontal velocity is 0.1 and for the vertical velocity is 0.2. All velocities are scaled by the intrusion front speed and Benjamin's energy-conserving shape is plotted as a dashed line.

to the intrusion head, the velocities are nearly uniform and significantly weaker, with speeds within approximately 10% of U_f.

The vertical velocity contours (figure 5*c*,*d*) show that there is little vertical motion within the head region. Further behind, near $x/H \approx 1.5$, however, there are regions of high vertical velocities with maximum velocities on the order of 50% of the front speed. These high vertical velocities are found in positive and negative pairs and correspond to the billows in the wake of the intrusion. Similar horizontal and vertical velocity contour plots were obtained for all other runs, and the core of high-velocity fluid appeared to increase slightly in strength as the Reynolds number was increased.

https://doi.org/10.1017/S0022112001007303 Published online by Cambridge University Press

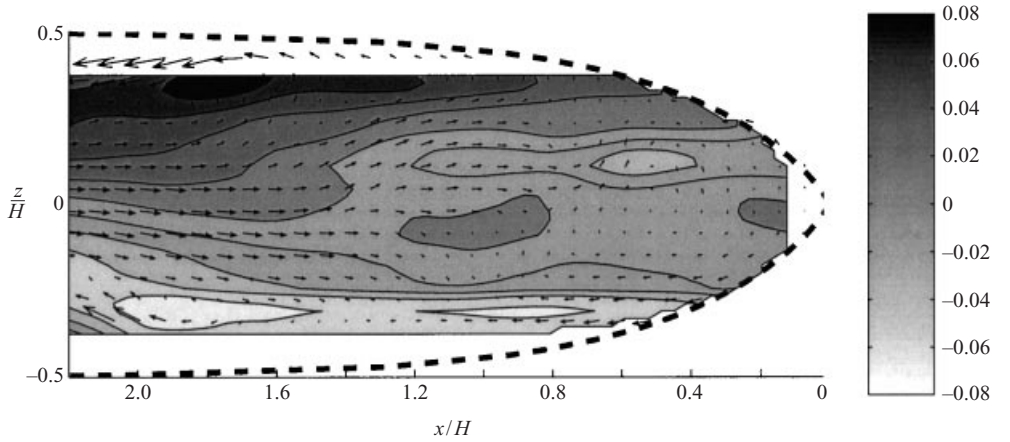


FIGURE 6. The velocity field inside the intrusion in Run D ($Re_H = 6400$), measured using PTV. The arrows represent fluid velocity (the length of the arrow on the left boundary at $z/H = 0$ has a magnitude of 0.46 U_f). The contours are lines of constant streamfunction non-dimensionalized by $U_f H$ and plotted at a contour interval of 0.012. The dashed lines represent Benjamin's energy-conserving current shape.

Figure 6 is a velocity vector plot of the flow field in the intrusion head for Run D ($Re_H = 6400$), in a frame of reference moving with the current front. The data have been time-averaged over 1.5 s using velocity data sampled every 0.25 s. Contours of the instantaneous streamfunction are also shown. The dominant features of the flow are the two vortices visible in the upper and lower parts of the intrusion at $x/H \approx 1.8$. A comparison with the corresponding shadowgraph image in figure 7(*a*) shows that these vortices correspond to the largest billows. These vortices roll up and advect fluid away from the centreline and entrain ambient fluid. When the billows subsequently collapse, the resulting mixed fluid has lost its forward momentum and is left behind in the wake. As a result, the diluted fluid mixture does not penetrate into the intrusion head. This velocity structure explains why Hallworth *et al.* (1996) and Hacker *et al.* (1996) observed that the dense fluid within the head of a gravity current remains largely undiluted throughout the constant velocity phase.

The core of high-velocity fluid behind the largest billows supplies the dense fluid lost by mixing. The relative velocities are much smaller in front of the billows, and more closely match the front speed. This velocity structure explains why Benjamin's energy-conserving model works so well for full-depth lock-release gravity currents with energy dissipation in the wake. In the head region, Benjamin's energy-conserving assumptions are indeed justified because the flow field is close to uniform and the dense fluid driving the motion remains largely undiluted. The fluid in the gravity current head propagates as a nearly uniform region of fluid, largely insensitive to the dissipation in the wake.

Benjamin's (1968) theoretical shape for an energy-conserving gravity current (see his §4.3, equations (4.32–33)) is plotted as a dashed line on the shadowgraph image in figure 7. It provides an accurate representation of the intrusion head, which further illustrates the robust nature of Benjamin's energy-conserving solution. The intrusion departs from Benjamin's shape in the wake region, which forms behind the intrusion head as the billows collapse into three-dimensional small-scale turbulence. In this wake region, the intrusion thickness appears constricted in the vertical direction, presumably due to the high forward velocities which reduce the pressure within the

https://doi.org/10.1017/S0022112001007303 Published online by Cambridge University Press

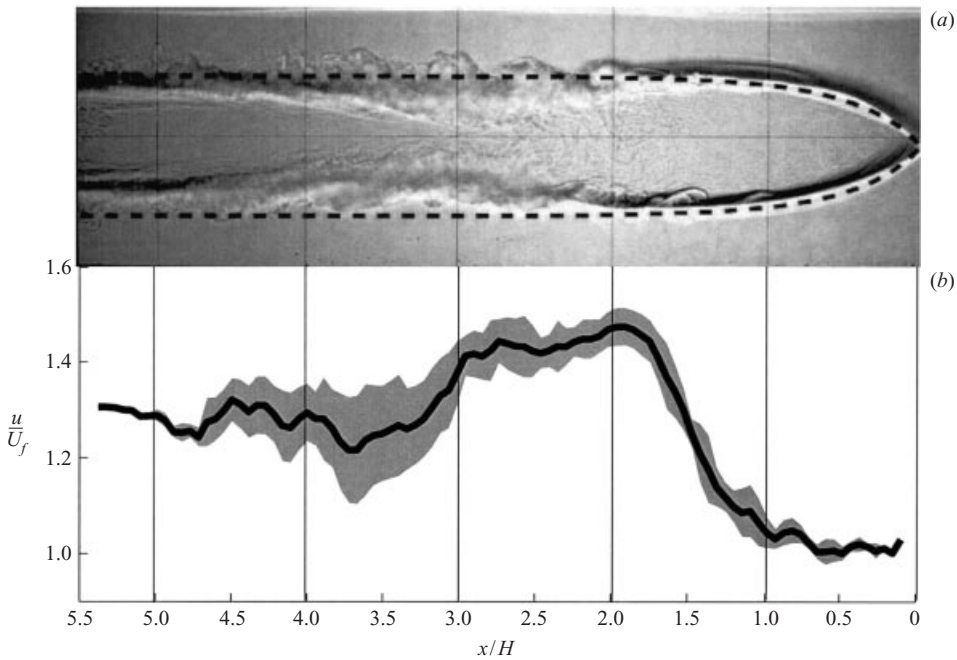


FIGURE 7. (*a*) A shadowgraph image of the intrusion in Run H ($Re_H = 6700$). Benjamin's energy-conserving current shape is plotted as a dashed line; (*b*) the horizontal component of fluid velocity on the intrusion centreline as a function of x, the distance behind the front, for Run D ($Re_H = 6400$). The standard deviation for this measurement is indicated by the shaded region.

intrusion and constrict the interface. Despite the obvious energy losses behind the head, these experiments show that the head of a lock-release gravity current behaves like an energy-conserving gravity current, and that the head is largely insensitive to the complicated flow patterns in the wake.

The centreline horizontal velocity u along the intrusion centreline, non-dimensionalized with U_f, is plotted against the distance behind the front x/H in figure 7(*b*), beneath the shadowgraph image of the corresponding flow with almost identical Re_H. From $x/H \approx 0$ to 1.5 the horizontal velocity component closely matches the front speed and there is little flow relative to the front. After $x/H \approx 1.5$ the velocity increases and attains a maximum velocity approximately 50% greater than the front speed at $x/H \approx 2$. Comparison with the shadowgraph image reveals that this maximum velocity occurs at the location where the strongest billows occur. Beyond $x/H \approx 3$ the velocity decreases until a near uniform velocity approximately 30% greater than the front speed is attained as the interface restabilizes downstream.

It is interesting to note that Kneller, Bennett & McCaffrey (1999) found a similar velocity structure in their measurements in a boundary gravity current, which had a comparable Reynolds number to our experiments. Using laser Doppler anemometry they found that the maximum velocity in their gravity current was 51% greater than the front speed and occurred at a distance $x/H \approx 1.2$ behind the front. The magnitude of this maximum velocity is nearly the same as the measured values in our experiments and the horizontal position is close to our value. A small difference with our experiments is that they found this maximum velocity occurred at a height $z \approx 0.2h$ above the no-slip boundary, where h is the current height, whereas in our experiments this maximum velocity occurred on the centreline.

https://doi.org/10.1017/S0022112001007303 Published online by Cambridge University Press

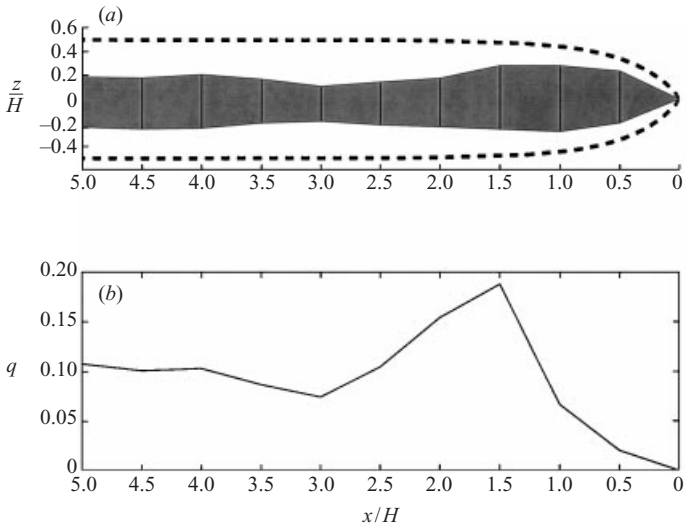


FIGURE 8. The time-averaged volume flux structure for Run F. (*a*) The region in the flow (shaded in grey) here the horizontal velocities are moving faster than the front speed. The vertical solid lines indicate the sections where the flux was calculated and Benjamin's energy-conserving shape is plotted as a dashed line. (*b*) The dimensionless volume flux $q = Q/U_f H$, where Q is defined by (4.1), is plotted versus the distance behind the intrusion front.

4.3. *Volume fluxes*

The horizontal volume flux was calculated for Run F at several vertical cross-sections in the flow. The volume flux Q per unit width of the tank was computed by integrating along vertical sections of the flow where the velocities are moving faster than the front speed, such that

$$Q = \int_{d_1}^{d_2} [u(x,z) - U_f]\,\mathrm{d}z. \tag{4.1}$$

The limits d_1 and d_2 represent the heights above and below the intrusion centreline, respectively, where the horizontal velocities $u(x,z)$ are moving faster than the front. The shaded region in figure 8(*a*) indicates the region in the flow where u is greater than the front speed and the vertical solid lines indicate the 10 equally spaced vertical sections where Q was calculated. The volume fluxes were time-averaged for 3.67 s using data sampled every 1/6 s.

The dimensionless volume flux $q = Q/U_f H$ of fluid within the intrusion is plotted against the distance behind the intrusion front x in figure 8(*b*). The volume flux is nearly constant at $q \approx 0.1$ far downstream in the region from $x/H \approx 3$ to 5. In the turbulent wake region from $x/H \approx 1.5$ to 3, where the billows break down, q increases, attaining a maximum of $q \approx 0.2$ at $x/H \approx 1.5$. Although an increase in the volume flux appears to violate volume conservation, it is important to recognize that the volume fluxes are computed by integrating over the region in the flow where the fluid is moving forward relative to the front. As a result, the increase in the volume flux is due to entrainment of ambient fluid. If we had measured the velocity in the ambient fluid layers it would be possible to integrate over the entire depth of the fluid in the tank, in which case we would expect volume to be conserved.

From $x/H \approx 1$ to 1.5 the volume flux decreases dramatically, as nearly 75% of the volume flux at $x/H \approx 1.5$ is detrained and never reaches the front. Comparison with

https://doi.org/10.1017/S0022112001007303 Published online by Cambridge University Press

the velocity structure for Run F in figure 5 shows that the strongest billows emerge at $x/H \approx 1.75$, and produce the strongest vertical velocities at this location. As these billows roll up, they draw fluid at $x/H \approx 1.5$ away from the centreline and little excess flux reaches the front.

Simpson & Britter (1979), using their stationary gravity current apparatus, measured an 'overtaking speed' U_o, which they defined as the mean velocity of the dense fluid supplying the gravity current. They determined U_o indirectly by measuring the flux Q per unit width of the dense fluid needed to arrest the front and assuming that the flow in the wake has both uniform velocity U_o and depth d. This gives $U_o = Q/d$, which they measured to be $U_o/U_f = 0.16 \pm 0.04$ in their experiments. The overtaking speed U_o was determined for Run F using the relationship $U_o/U_f = qH/d$. The mean height of the wake d measured far downstream was $d/H = 0.44 \pm 0.04$, and the dimensionless flux $q \approx 0.1$. Hence, the overtaking speed was determined to be $U_o/U_f = 0.23 \pm 0.05$ which is similar to the value obtained by Simpson & Britter (1979).

It is important to mention that this overtaking speed is often cited as the flow speed within the wake of a gravity current even though Simpson & Britter (1979) comment that it is possible for the maximum internal velocity to be larger. Our measurements show that the overtaking speed is less than half of the maximum internal velocity, and to use a single overtaking speed to describe the flow within the gravity current does not capture the complexity of the structure.

4.4. *Comparison with direct numerical simulations*

Härtel *et al.* (2000) performed DNS of Boussinesq lock-release gravity currents flowing over both no-slip and slip (stress-free) boundaries. They carried out two-dimensional simulations over a range of Reynolds numbers $Re_{H'}$, based on the total depth H', between 240 and 64 000, and a single three-dimensional simulation with no-slip boundary conditions at $Re_{H'} = 1500$. The length scale H' is equivalent to the layer depth H for a symmetric lock-release intrusion, since an intrusion is equivalent to a pair of boundary gravity currents, one a reflection of the other about the interface (Britter & Simpson 1981). The results of their simulations for gravity currents over slip boundaries can be directly compared to the intrusions discussed in this paper, which similarly exclude the effects of a no-slip boundary.

The simulations display most of the features observed in laboratory lock-release gravity currents, including interfacial billows behind the gravity current head. They found that these billows first emerge at a distance $x/H' = 2.5$ to 4 behind the front, which is comparable to (although larger than) the distance $x/H = 1.5$ to 2.5 we observed in the shadowgraph images. The most notable difference is that, in their two-dimensional simulations, the vortices cannot break down into small-scale three-dimensional turbulence, which is precluded in a two-dimensional model, and the billows subsequently continue to persist and grow in the wake of the current, attaining physically unrealistic amplitudes. Figure 9(a) shows a two-dimensional simulation visualized by isopycnal contours for a gravity current at $Re_{H'} = 4800$ advancing over slip boundaries. Comparison with the intrusion shadowgraph image in figure 7 shows that in laboratory gravity currents the billows rapidly break down into three-dimensional small-scale turbulence and vanish downstream as the interface restabilizes.

Although the billows fail to break down in the two-dimensional simulations, Härtel *et al.* (2000) note that the front speeds from their two-dimensional simulations are in close agreement with the result from their three-dimensional simulation, implying that

https://doi.org/10.1017/S0022112001007303 Published online by Cambridge University Press

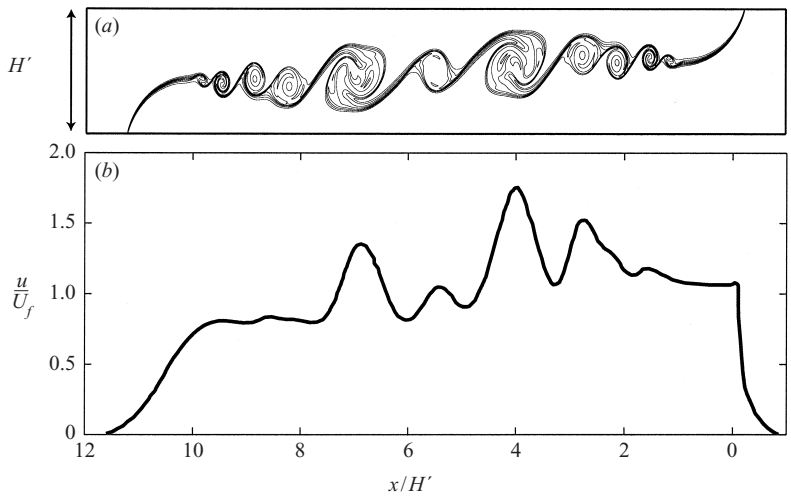


FIGURE 9. Two-dimensional lock-exchange DNS with slip boundaries. (*a*) The flow structure visualized by isopycnal contours. (*b*) The longitudinal profile of the horizontal velocity component along the upper boundary (Härtel, private communication).

the front speed is not dependent on three-dimensional effects. Moreover, for flows along slip boundaries above a sufficiently high Reynolds number, the dimensionless front speed approaches $U_f/(g_0'H')^{1/2} = 0.49$. This value is within 2% of the energy-conserving value, and closely matches the front speeds in our experiments (see table 1). Härtel *et al.* (2000) superimposed Benjamin's (1968) theoretical energy-conserving shape on their simulations and observed a near perfect match at the current head, further supporting our suggestion that the head of a gravity current conserves energy during its constant speed phase.

Figure 9(*b*) shows the horizontal velocity component u plotted along the upper shear-free boundary for the two-dimensional simulation shown in figure 9(*a*). From $x/H' \approx 0$ to 2, in the head where the interface is stable, the velocity is nearly constant at the front speed. Behind this constant speed region, the velocity increases with increasing distance behind the front and then oscillates, attaining local maxima at $x/H' \approx 3$ and $x/H' \approx 4$, with magnitudes of approximately 50% and 70% greater than the front speed, respectively. Figure 9(*a*) reveals that these peaks occur directly below the largest billows, which is consistent with our experiments. In front of these billows, where the interface is stable, the velocity is constant, which is consistent with our observations.

The obvious difference between the experimental velocity profiles (figure 7) and the two-dimensional simulations is that the latter show multiple velocity peaks, while our measurements have only a single peak. As mentioned above, this discrepancy results from the fact that in the two-dimensional simulations the billows cannot collapse into small-scale turbulence and their effects on the velocity structure persist and grow in the wake. Our experiments show that these billows break down upon reaching a finite size and gradually lose their vorticity. As a result, there is a single velocity peak where the billows have attained their largest size immediately before they start to break down. It is, therefore, not surprising that the shape of the velocity profile in figure 9(*b*) is nearly identical to the experimental profile in figure 7, only in the frontal region extending from the front of the current to the first velocity peak. In the two-dimensional simulation the initial velocity peak has a magnitude about 50% greater

https://doi.org/10.1017/S0022112001007303 Published online by Cambridge University Press

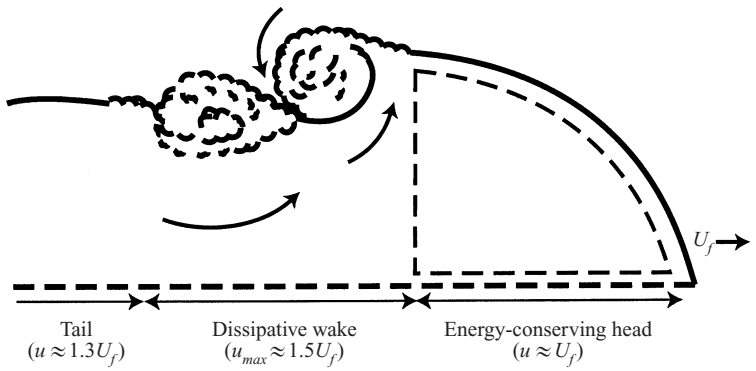


FIGURE 10. Schematic representation of the two-dimensional flow structure within a symmetric intrusion, in which u represents the fluid velocity within the current. Only the upper half of the intrusion is shown; the intrusion is assumed to be symmetric about the thick horizontal dashed line.

than the front speed, in good agreement with the maximum velocities observed in our experimental measurements. The larger secondary peak, with a magnitude about 70% greater than the front speed, is not observed in our experiments, because the billow responsible for this maximum would have collapsed due to a three-dimensional instability. We would expect much closer agreement in the wake region, however, if we could compare our results to the three-dimensional DNS in Härtel *et al.* (2000), but unfortunately this simulation has no-slip boundary conditions and does not include any longitudinal velocity profiles to compare with our experimental measurements.

5. Summary and conclusions

These experiments reveal a velocity structure within a full-depth lock-release intrusive gravity current that is quite different from the currently accepted picture. Previous gravity current models (see Simpson 1997) assume that dense fluid at the rear of a gravity current travels faster, and reaches the nose of the current and returns back towards the wake along the shear interface separating the dense and ambient fluid layers. Although these experiments reveal that some of the dense fluid at the rear of the intrusion reaches the front, most of the dense fluid is advected away from the centreline due to the billows, and never reaches the front. A more appropriate gravity current front model is presented in figure 10, which divides the current into three distinct regions. At the front of the intrusion there is an energy-conserving head region in which the fluid velocity is nearly uniform with speed equal to the front speed. This is followed by a dissipative wake region in which large billows are present with their associated mixing and in which the fluid velocity is observed to be non-uniform and with maximum speed approximately 50% greater than the front speed. Behind the wake region is a tail region in which there is very little mixing and the velocity field is nearly uniform with a speed slightly faster than the front speed.

The maximum velocity was found to be approximately 50% greater than the front speed and occurred near the position in the intrusion where the largest billows form. In this region, the fluid within the intrusion is detrained into the wake, so velocities higher than the front speed are required to balance the mass lost through mixing. The diluted fluid mixture in the wake does not penetrate into the head of the intrusion, which explains why a gravity current head does not dilute significantly during its constant speed phase.

https://doi.org/10.1017/S0022112001007303 Published online by Cambridge University Press

Benjamin's energy-conserving analysis assumes that there is no relative flow within the head of a gravity current. Our measurements reveal that this is a good approximation: horizontal velocities were found to be no greater than about 10% of the front speed. Hence, the kinetic energy of the internal circulation is less than approximately 20% of the total kinetic energy in the head, which explains why it can be neglected in the theory. We conclude, therefore, that intrusions generated by a lock-release – and by implication gravity currents travelling along a slip boundary – for Reynolds numbers in the range 3700–14 500, are well described by Benjamin's energy-conserving theory. The speed and the shape of the current agree well with the theory, despite the fact that dissipation is observed behind the head. This supports the notion that the flow is controlled at the head, and the dynamics are essentially energy-conserving there.

Isao Kanda provided extensive help with DigImage and the PTV technique. Alison Newkirk and Victoria Arrigoni, undergraduate students in the MAE Department at UCSD, assisted with the experiments and the analysis of the data. We thank Carlos Härtel, Eckart Meiburg and Frieder Necker for providing us with the results of their numerical simulations shown in figure 9.

Appendix. Effect of the density ratio

In the environment density differences are rarely higher than a few percent and the Boussinesq approximation is valid. But for many industrial flows higher density ratios are common. For these non-Boussinesq cases there are no analytical solutions to the governing equations, which led Holyer & Huppert (1980) to obtain numerical solutions. However, for weakly non-Boussinesq fluids we can use perturbation methods to determine an approximate solution. Using the nomenclature defined in § 2, we define an expansion parameter $\epsilon \geqslant 0$ such that

$$\gamma^{-1} = \frac{\rho_2}{\rho_0} = 1 + 2\epsilon. \tag{A 1}$$

The reduced gravities are then expressed as

$$\frac{g_0'}{g} = \epsilon, \qquad \frac{g_2'}{g} = \epsilon - 2\epsilon^2 + O(\epsilon^3). \tag{A 2}$$

Using the intrusion height ratios found for a symmetric Boussinesq intrusion we assume an expansion of the form

$$\frac{h_0}{H} = \tfrac{1}{2} + a\epsilon + O(\epsilon^2), \quad \frac{h_2}{H} = \tfrac{1}{2} + b\epsilon + O(\epsilon^2) \tag{A 3}$$

for the current heights in a weakly non-Boussinesq intrusion. The coefficients a and b are determined by substituting (A 2) and (A 3) into the momentum conservation equation (equation (7) in de Rooij *et al.* 1999). Equating (2.1) and (2.2) gives the following relations for the intrusion front speed and current heights:

$$\frac{U_f}{\sqrt{g_0' H}} = \tfrac{1}{2} - \tfrac{1}{4}\epsilon + O(\epsilon^2), \tag{A 4}$$

$$\frac{h_0}{H} = \tfrac{1}{2} + \tfrac{3}{8}\epsilon + O(\epsilon^2), \tag{A 5}$$

$$\frac{h_2}{H} = \tfrac{1}{2} - \tfrac{3}{8}\epsilon + O(\epsilon^2). \tag{A 6}$$

https://doi.org/10.1017/S0022112001007303 Published online by Cambridge University Press

Equations (A 5)–(A 4) show that the effect of perturbing the density ratio away from the Boussinesq limit is to decrease the dimensionless front speed and to make the intrusion asymmetric about the upstream interface. The intrusion is shifted up by a small amount, although the total thickness of the intrusion stays the same (to this approximation) as that of the Boussinesq intrusion. The upper limit for ϵ in these experiments is 0.09 (see table 1), which according to (A 4) corresponds to a decrease in Fr by about 4%, consistent with our measurements. This confirms that the Boussinesq solution given in (2.6) gives a reasonable approximation over the full range of experiments reported in this paper.

REFERENCES

Benjamin, T. B. 1968 Gravity currents and related phenomena. *J. Fluid Mech.* **31**, 209–248.

Britter, R. E. & Simpson, J. E. 1981 A note on the structure of an intrusive gravity current. *J. Fluid Mech.* **112**, 459–466.

Faust, K. M. & Plate, E. J. 1984 Experimental investigation of intrusive gravity currents entering stably stratified fluids. *J. Hydraul. Res.* **22**, 315–323

Hacker, J., Linden, P. F. & Dalziel, S. B. 1996 Mixing in lock-release gravity currents. *Dyn. Atmos. Oceans* **24**, 183–195.

Hallworth, M. A., Huppert, H. E., Phillips, J. C. & Sparks, R. S. J. 1996 Entrainment into two-dimensional and axisymmetric turbulent gravity currents. *J. Fluid Mech.* **308**, 289–311.

Härtel, C., Meiburg, E. & Necker, F. 2000 Analysis and direct numerical simulation of the flow at a gravity-current head. Part 1. Flow topology and front speed for slip and no-slip boundaries. *J. Fluid Mech.* **418**, 189–212.

Holyer, J. Y. & Huppert, H. E. 1980 Gravity currents entering a two-layer fluid. *J. Fluid Mech.* **100**, 739-767.

Huppert, H. E. & Simpson, J. E. 1980 The slumping of gravity currents. *J. Fluid Mech.* **99**, 785–799.

Kneller, B. C., Bennett, S. J. & McCaffrey, W. D. 1999 Velocity structure, turbulence and fluid stresses in experimental gravity currents. *J. Geophys. Res.* **104**, 5381–5391.

de Rooij, F., Linden, P. F. & Dalziel, S. B. 1999 Saline and particle-driven interfacial intrusions. *J. Fluid Mech.* **389**, 303–334.

Rottman, J. W. & Simpson, J. E. 1983 Gravity currents produced by instantaneous releases of a heavy fluid in a rectangular channel. *J. Fluid Mech.* **135**, 95–110.

Simpson, J. E. 1997 *Gravity Currents in the Environment and the Laboratory*, 2nd Edn. Cambridge University Press.

Simpson, J. E. & Britter, R. E. 1979 The dynamics of the head of a gravity current advancing over a horizontal surface. *J. Fluid Mech.* **94**, 477–495.

https://doi.org/10.1017/S0022112001007303 Published online by Cambridge University Press